

The Very Early Light Curve of SN 2015F in NGC 2442: A Possible Detection of Shock-Heated Cooling Emission and Constraints on SN Ia Progenitor System

Myungshin Im^{1,2,6}, Changsu Choi^{1,2,6}, Sung-Chul Yoon², Jae-Woo Kim^{1,2}, Shuhrat A. Ehgamberdiev³, Libert A. G. Monard⁴, & Hyun-Il Sung⁵

¹*Center for the Exploration of the Origin of the Universe (CEOOU), Seoul National University, Seoul, Republic of Korea*

²*Astronomy Program, Department of Physics & Astronomy, Seoul National University, Seoul, Republic of Korea*

³*Ulugh Beg Astronomical Institute, Tashkent, Uzbekistan*

⁴*Kleinkaroo Observatory, Center for Backyard Astrophysics Kleinkaroo, Sint Helena 1B, PO Box 281, Calitzdorp 6660, South Africa*

⁵*Korea Astronomy and Space Science Institute, Daejeon 305-348, Republic of Korea*

⁶mim@astro.snu.ac.kr, changsu@astro.snu.ac.kr

ABSTRACT

The main progenitor candidate of Type Ia supernovae (SN Ia) is white dwarfs in binary systems where the companion star is another white dwarf (double degenerate system) or a less evolved non-degenerate star with $R_* \gtrsim 0.1 R_\odot$ (single degenerate system), but no direct observational evidence exists that tells which progenitor system is more common. Recent studies suggest that the light curve of a supernova shortly after its explosion can be used to set a limit on the progenitor size, R_* . Here, we report a high cadence monitoring observation of SN 2015F, a normal SN Ia, in the galaxy NGC 2442 starting about 84 days before the first light time. With our daily cadence data, we catch the emergence of the radioactively powered light curve, but more importantly detect with a $> 97.4\%$ confidence a possible dim precursor emission that appears at roughly 1.5 days before the rise of the radioactively powered emission. The signal is consistent with theoretical expectations for a progenitor system involving a companion star with $R_* \simeq 0.1 - 1 R_\odot$ or a prompt explosion of a double degenerate system, but inconsistent with a typically invoked size of white dwarf progenitor of $R_* \sim 0.01 R_\odot$. Upper limits on the precursor emission also constrain the progenitor size to be

$R_* \lesssim 0.1 R_\odot$, and a companion star size of $R_* \lesssim 1.0 R_\odot$, excluding a very large companion star in the progenitor system. Additionally, we find that the distance to SN 2015F is 23.9 ± 0.4 Mpc.

Subject headings: supernovae: general — supernovae: individual (SN 2015F) — white dwarfs — galaxies: distances and redshifts

1. INTRODUCTION

Explosive death of a star, supernova, is a dramatic cosmic event that occurs at the end of the evolutionary path of many stars. Observational study of such events can tell us whether our theoretical understanding of stellar evolution is correct, and thus studies of supernovae have been actively pursued ever since modern astronomy has begun.

Among various kinds of supernovae, SNe Ia are believed to be the thermonuclear explosion of carbon-oxygen (C/O) white dwarfs in close binary systems (see Maoz et al. 2014 for a recent review on this subject). This scenario is supported by the energetics and the chemical composition of the ejecta, as well as the progenitor ages inferred from their host galaxy properties (Holye & Fowler 1960; also see Hillebrandt & Niemeyer 2000). Yet we have no direct observational evidence that can constrain their progenitor systems, such as the size of the exploding star and the nature of its companion. Two progenitor systems are theorized. One is the Single Degenerate (SD) system where the companion star is a non-degenerate star with a radius of $0.1 - 100 R_\odot$ depending on its mass and evolutionary stage. The other is the Double Degenerate (DD) system where two white dwarfs merge to produce a SN Ia in a close binary system as a result of orbital angular momentum loss via gravitational wave radiation. In both cases, the size of the exploding white dwarf is expected to be small ($\lesssim 0.01 R_\odot$). However, in the SD system, if the white dwarf was a recurrent nova that accretes hydrogen-rich material with a fairly high mass accretion rate ($dM/dt \sim 10^{-6} M_\odot/\text{yr}$), the radius of the envelope could be as large as $0.2 R_\odot$ (e.g., Hachisu & Kato 2003). In the DD scenario, the radius of the shock breakout surface would be about $0.1 R_\odot$ if a prompt detonation occurred as a result of the merger (Pakmor et al. 2012; Tanikawa et al. 2015), while in the case of a long-delayed ($> 10^4$ yr) explosion after the merger, the radius would be only about $0.01 R_\odot$ (Yoon et al. 2007).

It has been suggested that the very early light curve within ~ 1 day of the explosion can constrain properties of the progenitor system such as the radius of the detonating star and the companion star (Nakar & Sari 2010; Piro et al. 2010; Kasen 2010, hereafter, K10; Rabinak & Waxman 2011, hereafter RW11; Maeda et al. 2014; Kutsuna & Shigeyama

2015). This is because the luminosity from the shock-heated materials that immediately follows the shock breakout is proportional to the radius of the progenitor star for a given set of progenitor mass and the supernova explosion energy (K10; Piro et al. 2010; RW11; Rabinak et al. 2012; Piro & Nakar 2013, 2014; Pan et al. 2012). This phase has been shown to last for several hours or more, with the exact duration depending on the progenitor size (Rabinak et al. 2012; Piro & Nakar 2013). The emission is generally dim with $M_R \sim -10 - -14$ mag for a progenitor radius of $0.1 - 1 R_\odot$ (Figure 3), but it could be much brighter if a much larger star is involved ($M_R \sim -17$ mag for $100 R_\odot$; K10).

Recently, several SNe Ia have been discovered in very early phases (SN 2009ig: Foley et al. 2012; SN 2011fe: Nugent et al. 2011; SN 2012cg: Silverman et al. 2012; SN 2012ht: Yamanaka et al. 2014; SN 2013dy: Zheng et al. 2013; SN 2014J: Zheng et al. 2014; Goobar et al. 2014; Olling et al. 2015; Shappee et al. 2015), providing light curves within $\sim 1 - 2$ day of the first light time¹ and providing an opportunity to constrain the progenitor star radius. In general, studies involving early light curves of normal SNe Ia suggest small progenitor sizes. Using SN 2011fe, Nugent et al. (2011) constrained the progenitor radius, R_* , to be $R_* < 0.1 R_\odot$, while Bloom et al. (2012) suggested an even tighter constraint of $R_* < 0.02 R_\odot$ based on a non-detection at 7.5 hours before the estimated first light time. Similar attempts have been made using other SNe Ia with early light curves, giving the limits of $R_* < 0.25 - 0.35 R_\odot$ for SN 2013dy (Zheng et al. 2013), $R_* < 1.5 - 2.7 R_\odot$ for SN 2012ht (Yamanaka et al. 2014), and $R_* < 0.34 R_\odot$ for ASASSN-14lp (Shappee et al. 2015). Similar limits are given for three SNe Ia from the *Kepler* mission (Olling et al. 2015). On the other hand, Goobar et al. (2015) suggest that a progenitor system with a scale of $R \gtrsim 1 R_\odot$ for SN 2014J. For iPTF14atg, Cao et al. (2015) find an early UV light that is consistent with a system that has a large companion star (several tens of R_\odot). However, the SN studied in Cao et al. (2015) is an underluminous SN Ia, a peculiar one. We also note a possible detection of a single progenitor system for SN 2012Z, another underluminous SN Ia (type Iax), in a pre-explosion image (McCully et al. 2014).

These results assumed that the explosion time of SNe Ia coincides with the first light time of the light curve that is dominated by the heating due to radioactive decay of ^{56}Ni . However, the rise of the radioactively powered light curve is expected to start a few hours to a few days after the explosion depending on how deep the ^{56}Ni layer is (Piro & Nakar 2013), while the UV/optical emission from shock-heated materials occurs almost immediately after the explosion (e.g., Höflich & Schaefer 2009). Hence, the previous constraints on SNe Ia

¹We use the term, “first light time”, to indicate when the radioactively powered light curve started to rise, and we distinguish the first light time from the actual explosion time at around the shock breakout (e.g., Piro & Nakar 2013).

progenitors have been put into question. This time gap between the thermonuclear explosion and the rise of the radioactively powered light curve has been called as “dark phase” or “delay time” which we note as t_d for convenience. The analysis of the early spectra of SN 2011fe by Mazzali et al. (2014) led them to conclude that the actual explosion of SN 2011fe preceded about 1 day before the first light time estimated by Nugent et al. (2011). The inclusion of the uncertainty in the duration of the dark phase weakens the limits on the progenitor star radius to $R_* \lesssim 0.1R_\odot$ for SN 2011fe (Piro & Nakar 2014; Mazzali et al. 2014).

The uncertainties in the estimate of the explosion time and t_d can be reduced by utilizing high cadence non-detection data going back to several days prior to the first light time. For example, Mazzali et al. (2014) combined their estimate of the explosion time and the non-detection of SN 2011fe around that time, and put forward a constraint of $R_* < 0.06 R_\odot$. This, however, depends on the accuracy of the explosion time estimate again, and the constraint on R_* could be weaker if the SN 2011fe explosion occurred even before their estimate. Unfortunately, there is a general lack of high cadence data prior to the first detection² of SNe, so that a study similar to this is not possible for the majority of SNe. Ultimately, a direct detection of the emission from shock-heated cooling prior to the first light time can lead to a very tight constraint on both the explosion time and the progenitor property.

SN 2015F was discovered by one of us (Monard) in NGC 2442 on 2015 Mar.09.789 (UT) in its early phase, and has been classified as a SN Ia (Fraser et al. 2015). The data from our regular monitoring program, Intensive Monitoring Survey of Nearby Galaxies (IMSNG), of NGC 2442 show a pre-discovery detection at 2015 Mar.08.46. We have been monitoring NGC 2442 on a daily basis from 2014 December 14, and the data reveal positive signals at Mar.05.57 and Mar.6.55 that we interpret as an emission from shock-heated materials as we show below. In this paper, we will make use of these high cadence data to place constraints on the SN Ia progenitor size. In addition, we will derive the distance modulus of NGC 2442 and the properties of SN 2015F.

2. OBSERVATION

IMSNG is a high cadence imaging survey monitoring nearby galaxies to catch transients such as SNe in their early phases. The final goal of the survey cadence is 3 hrs, using a network of telescopes all over the world. We started our test observations in 2013B with a 1m telescope at Mt. Lemmon Optical Astronomy Observatory in US, SNUCAM on the 1.5m

²Throughout this paper, we use the term “first detection” to indicate the first detection of the radioactively powered light curve.

telescope at Maidanak observatory in Uzbekistan (Im et al. 2010), and a 0.6m telescope of Mt. Sobaek Optical Astronomy Observatory in Korea. In 2014 October, we installed a 0.43m telescope (Lee Sang Gak Telescope, LSGT hereafter; Im et al. 2015) at the Siding Spring Observatory, Australia, which enabled us to perform a few hours to daily cadence observation of nearby galaxies that are accessible in the southern hemisphere. Since 2014 December 14, R -band images of NGC 2442 have been taken once to three times every night at a ~ 1.5 hour interval (weather permitting), using SBIG ST-10XME camera on LSGT which provides a field of view of $17'.5 \times 11'.8$ and a pixel scale of $0''.48$. Three frames, each with 180 s exposure, have been taken at a given epoch. Occasionally, B -band and V -band observations were added. Typical seeing full-width-half-maximum (FWHM) values ranged between $1''.8$ to $4''.0$ with a medium value at $2''.5$ (Im et al. 2015). The LSGT data were reduced with a standard procedure of dark subtraction and flat-fielding as soon as the data were taken.

During the monitoring observation, the emergence of SN 2015F was recorded in the LSGT images taken at 2015 Mar. 08.46, 09.54, and 11.50 (Figure 1). In comparison, we show an image taken at 2015 Mar. 07.52, approximately one day before the first detection of SN 2015F. To better identify the SN by subtracting a reference image, we constructed a master reference image using the LSGT data taken during 2015 January to February under good weather conditions. The reference image was convolved with a Gaussian profile and flux-scaled to match the seeing and the zero-point of each epoch image. And then, the reference image was subtracted to yield a difference image. Some LSGT data had better seeing than the reference image. In such cases, we convolved the later epoch data to match the reference image resolution. The subtraction of the reference image removes NGC 2442 effectively, allowing us to see SN 2015F clearly.

The photometry calibration was done using calibration stars from the data release 8 (DR8) of the AAVSO photometric all-sky survey (APASS; Henden et al. 2012). The B and V -band data were taken directly from APASS values, and the R -band values of calibration stars were obtained by converting APASS r and i -band photometry to the Johnson R -system using a SDSS photometry transformation equation in the form of $R = r - 0.2936 \times (r - i) - 0.1439$ with a dispersion of $\sigma = 0.007$ mag. This procedure gives photometry zero-point for each epoch data, with a typical zero-point error of 0.02 mag. The photometry was done by running SExtractor (Bertin & Arnouts 1996) on images before (for calibration stars) and after (for SN 2015F) the subtraction of the reference image. We used $3''.0$ diameter aperture and applied an aperture correction that was derived from stars in the vicinity. The use of this size of aperture has an advantage of minimizing residual fluxes of extended features coming from an imperfect galaxy subtraction, if present. Upper limits at $3\text{-}\sigma$ are adopted for non-detections.

The discovery image and subsequent images of SN 2015F were also taken with a SBIG-ST8-XME camera (no filter) on Meade 12 or 14 inch RCX400 telescopes at the Kleinkaroo observatory in South Africa. Stacked images of three to four 13 s frames were used to search for SNe, and more than ten 13 s images were taken during the follow-up observation each night. The images were first calibrated with a standard reduction procedure of dark subtraction and flat-fielding and stacked to create a deeper image. An image of NGC 2442 taken before the SN detection was subtracted to create a difference image on which the photometry was performed in the same way as the LSGT data. For these data, color transformation equations were derived using $B - V$ colors of stars in the NGC 2442 field to convert the clear magnitudes to R -band magnitudes. The transformation equation has the form of $R = C_1 + C_2 \times (B - V)$. The C_1 and C_2 values were determined for each image and typical C_2 values are -0.1 and -0.23 for the 12 inch and 14 inch telescopes, respectively. For the $B - V$ color of the supernova, we first took the dereddened $B - V$ values of SN 2011fe at the same number of days from the B -band maximum (Richmond & Smith 2012), and then reddened them using the Galactic and internal (host galaxy) extinctions toward SN 2015F where the internal extinction comes from an analysis of the long term light curve fit (Section 3.1). The resulting $B - V$ values range from 0.58 (Mar.09) to 0.23 (Mar.15) mag. At the B -band maximum, the $B - V$ value estimated this way is 0.2 mag, which is in excellent agreement with the observed $B - V$ color of 0.2 mag for SN 2015F. Taking into account of the fitting error for the transformation equation and the uncertainty in $B - V$ (taken to be 0.1 mag), we get an uncertainty in the transformed R -band magnitude of 0.05 – 0.1 mag. Note that $B - V$ color could be redder by 0.3 mag in the early phase, since SN 2442 is not exactly identical to SN 2011fe (e.g., Yamanaka et al. 2014), but such an offset changes the resultant R -band magnitude only by 0.03 – 0.07 mag.

3. LIGHT CURVE ANALYSIS

3.1. Long-term Light Curve and Distance to SN 2015F

Figure 2 shows the long-term BVR light curve of SN 2015F up to 22 days after the B -band maximum. Also plotted are the light curves of SN 2011fe (Munari et al. 2013; Vinko et al. 2012; Richmond & Smith 2012). Here, the SN2011fe light curves are shifted in y-axis so that they correspond to the distance and the Galactic and internal extinctions of SN 2015F (Table 1). For SN 2011fe, we assumed the distance modulus of $\mu = 29.28^3$ (Lee & Jang

³Estimates of μ vary from 29.04 to 29.53 (Feldmeir et al. 1996; Macri et al. 2001; Sakai et al. 2004; Rizzi et al. 2007; Shappee & Stanek 2011; Richmond & Smith 2012; Vinko et al. 2012; Munari et al. 2013; Lee &

2012), the epoch of maximum brightness in B -band of $t_{\max}(B) = 2,455,815.00$ JD (average of t_{\max} from Vinko et al. 2012, Munari et al. 2013, Tsvetkov et al. 2013, and Pereira et al. 2013), the Galactic reddening of $E(B - V) = 0.008$ (Schlafly & Finkbeiner 2011), and the host reddening of $E(B - V)_{\text{host}} = 0.025$ (Patat et al. 2013). After adjustment, the light curves of SN 2011fe and SN 2015F match closely. This suggests that SN 2015F is a SN Ia very similar to SN 2011fe.

In order to characterize SN 2015F in more detail, we fitted the BVR light curve from LSGT with the MLCS2k2 model (Jha et al. 2007) using the SNANA software v10 (Kessler et al. 2009). The Galactic reddening of $E(B - V) = 0.179$ mag is adopted from Schlafly & Finkbeiner (2011; $A_R = 0.440$ mag, $A_B = 0.735$ mag, and $A_V = 0.556$ mag). The fit returns quantities such as the distance modulus and the host galaxy extinction (A_V), and other parameters such as Δ (the stretch factor in the MLCS2k2 model) and $t_{\max}(B)$.

The first two of these quantities, distance modulus and host galaxy extinction, play an important role in our analysis of the early light curves and constraining the progenitor size. Importantly, prior to this work, the distance to NGC 2442 has been poorly known, with published distance values varying from 17 Mpc (Tully 1988) to a more updated value of the distance modulus $\mu = 31.66 \pm 0.17$ (21.5 ± 1.7 Mpc) that is based on the group distance (Tully et al. 2009).

The fitting results are summarized in Table 1. The values and errors of the quantities such as $t_{\max}(B)$, Δ , B_{\max} (B magnitude at maximum brightness), and μ , are direct outputs from the SNANA software. Additionally, we derived other parameters by combining the SNANA output values with external information. The derived parameters are Δm_{15} (B magnitude difference between the maximum brightness and the brightness at 15 days after the maximum), $M_{B,\max}$ (absolute B magnitude at maximum brightness), t_{rise} (days between the first light time and $t_{\max}(B)$), and $E(B - V)_{\text{host}}$. Errors of these quantities are taken as the square root of the quadratic sum of errors of the quantities involved in the derivation. Note that when evaluating t_{rise} , we assumed a mid-point of first light times derived from two fitting methods (Section 3.2).

Our fitting gives the distance modulus of $\mu = 31.89 \pm 0.04$, the host galaxy reddening parameter of $E(B - V) = 0.035 \pm 0.033$ mag, $\Delta m_{15} = 1.26 \pm 0.10$, and $t_{\max} = 2,457,106.48 \pm 0.09$ JD (2015 Mar.24.98, UT). We conclude that the distance to NGC 2442 is 23.88 ± 0.40 Mpc, somewhat larger than previous estimates, and the dust-extinction by the host galaxy is small. The fitting results also confirm that SN 2015F is very similar to SN 2011fe which

Jang 2012; Tammann & Reindl 2013), and our adopted value of 29.28 corresponds roughly to a mid-point of these estimates.

has $\Delta m_{15} \simeq 1.1$ and $M_{B,\max} \sim -19.4$, showing that SN 2015F is a typical SN Ia.

3.2. Early Light Curve and First Light Epoch

Figure 3 shows the early light curve (-5 to +10 days after the first detection) of SN 2015F. Plotted along with the data points are the results from a single power-law fit (thick solid line), and a broken power-law fit (thin solid line), and the model predictions for the precursor emission from shock-heated materials (see below for the fitting functions and Section 4 for explanations for the models). Table 2 shows the photometry result of the early light curve from -84 days to 8 days. The values presented in Table 2 are not corrected for the Galactic extinction, which is $A_R = 0.44$ mag. The AB magnitude offset of 0.22 mag is used for the model prediction (e.g., Jeon et al. 2010).

The early light curve up to 8 days after the first detection was fitted with two functions. One is a single power-law $((t - t_0)^\alpha)$ where t_0 is the first light time with respect to the first detection epoch, and α is the power-law index. Another is a broken power-law function as given below (e.g., Zheng et al. 2013):

$$F(t) = F_0 \left[\left(\frac{t - t_0}{t_b} \right)^{\alpha_1} + \left(\frac{t - t_0}{t_b} \right)^{s(\alpha_1 - \alpha_2)} \right]^{-1/s}, \quad (1)$$

where F is the flux, F_0 is the normalization constant of the flux, t_b is the break time, α_1 and α_2 are the power-law indexes before and after the break, and s is a smoothing parameter. When $s = -1$, Eq. (1) reduces to a simpler broken power-law function that has been often used to model gamma ray burst afterglow (e.g., Urata et al. 2009). Zheng et al. (2013, 2014) show that a broken power-law function can fit the very early-light curve of SN 2013dy and SN 2014J, when there is a data point at ~ 0.5 days within the first light time.

The single power-law fit gives the result of $t_0 = 1.61 \pm 0.10$ days and $\alpha = 2.32 \pm 0.05$, with a reduced χ^2 value of $\chi_\nu^2 = 0.79$. When using a fixed value of $\alpha = 2$, we get $t_0 = 1.01 \pm 0.02$ days, but with $\chi_\nu^2 = 3.72$.

On the other hand, we find that the best-fit result of the broken power-law fit converges to the single power-law fitting result. This is because we cannot constrain α_1 and s values effectively due to the lack of a deep data point at $\lesssim 0.5$ days before our first detection. Even so, we can try to fit the existing data by fixing α_1 and s to the values obtained for another SN. Adopting the best-fit values of $\alpha_1 = 0.88$ and $s = -6.32$ of SN 2013dy (Zheng et al. 2013), we obtain $t_0 = 0.39 \pm 0.04$ days, $t_b = 1.98 \pm 0.06$ days, and $\alpha_2 = 1.89 \pm 0.02$ with $\chi_\nu^2 = 0.97$, which is a reasonably good fit. The broken power-law fitting result in Figure 3 uses these parameters. One can obtain $t_0 \sim 0.1$ day at $\chi_\nu^2 \sim 1.2$ by adopting $\alpha_1 \simeq 0.5$ and

$s \simeq -250$, although such a case produces a bumpy feature in the light curve near the first detection that looks artificial. These results suggest that the rise time is about 16.9 to 18.1 days.

We adopt the result of a single power-law fit for the following discussion, since it gives the best fit to our data. However, we should bear in mind that the first light time can be much smaller than the value inferred from the single power-law fit as was the case for SN 2013dy (Zheng et al. 2013) and SN 2014J (Goobar et al. 2014).

In the previous section, we mentioned that the uncertainty in $B - V$ color in the early light curve may cause a systematic offset of 0.03 – 0.07 mag through the transformation of clear magnitudes to R -band magnitude for the South African data. We find that the small offset in the photometry does not alter the fitting results much (well within the error estimates). This is because that the LSGT data are the most constraining data for the light curve fitting, and that the small systematic offset does not exceed errors of the South African photometry data points.

4. POSSIBLE DETECTION OF EMISSION FROM SHOCK-HEATED MATERIALS

To search for possible precursor UV/optical emission from shock-heated materials, we analyzed all the imaging data before the first detection that go back to 2014 December 14. The images taken at each night were stacked together to create a deeper image. Through this process, we created stacked images at 40 epochs before the first detection. An aperture photometry with a $3''0$ diameter was performed at the position of SN 2015F in the difference images at each epoch.

The result is presented in Figure 4. Interestingly, we find that the measurements from two epochs, at 3 and 2 days before the first detection, show weak but positive signals at $2-\sigma$ significance (or $R \sim 21$ AB mag). The significance of the combined signal from the two epochs is $3-\sigma$, and thus the formal probability of this being a true detection is 99.7%.

However, we caution that any unrecognized instrumental effects could produce a spurious signal at this level. Therefore, we varied our image reduction and analysis methods by choosing different sets of images to construct a reference image and performing additional flat-fielding using skyflats made from images of other targets observed during the same period. We also adopted various background annuli for the photometry. Even after these changes, the signal persisted at a similar statistical significance. We checked the detector temperatures during the monitoring observation, and we find them to be stable over the

course of the monitoring period, i.e., no anomaly in the detector temperature during these two nights. SN 2015F was placed at different locations on the chip in each time it was observed, but no hot/warm pixels or other detector defects were found in these positions including the Mar.05 and Mar.06 data.

Spurious, non-astrophysical signals can potentially be identified by examining source FWHM values. The FWHM values of astrophysical sources should be similar to those of stars in the same image. As a test, we inserted artificial stars at random locations in the images with the same flux as our potential detection and the seeing FWHM values that match the stellar FWHM values ($4''0$ and $2''6$ for Mar.05 and Mar.06 respectively). We find no significant difference between the injections and our detection in size or shape, although we caution that the test is not definitive in this case due to the low detection S/N.

Given that no $2\text{-}\sigma$ signal was detected over two consecutive nights in the other 38 consecutive epoch-pairs, we suggest that this is not a spurious signal. Based on the 39 consecutive epoch-pair measurements, we set a conservative probability of 2.6% (1/39) for two consecutive $2\text{-}\sigma$ detections occurring randomly at a particular time window. Therefore, we consider that the probability of this signal being real is $> 97.4\%$.

If the signal is due to the shock-heated cooling emission, the dark phase period corresponds to ~ 1.5 days. If the signal at $t \simeq -3$ days is due to a random coincidence, then the dark phase period would be ~ 0.5 days. Dark phase periods have been noted for SN 2010jn ($t_d=1.0$ day, Hachinger et al. 2013), SN 2009ig ($t_d \simeq 1.6$ day; Piro & Nakar 2014) and SN 2011fe ($t_d = 0.5$ to 1.5 day; Mazzali et al. 2014; Piro & Nakar 2014), with respect to the first light time estimates from a single power-law or a t^2 light curve. Therefore, the inferred dark period of $t_d \sim 1.5$ days is reasonable, given the dark phase estimates for the other SNe Ia and theoretical expectations.

To constrain the progenitor property with this possible shock-heated cooling signal, we use analytic models of the bolometric light curve and the temperature curve by RW11 and K10. The model of RW11 describes the evolution of the early shock-heated cooling emission from the progenitor itself, while the model of K10 is for the emission arising from an interaction between the companion star and the ejected materials. To model the R -band light curve, we used a black body radiation spectrum of a given effective temperature, and used the flux at the effective wavelength of R -band ($0.65 \mu\text{m}$).

For the RW11 model,

$$L(t) = 1.2 \times 10^{40} \frac{R_{10} E_{51}^{0.85}}{M_c^{0.69} r_{0.2}^{0.85} f_p^{0.16}} t_d^{-0.31} \text{ erg s}^{-1}$$

$$T_{eff}(t) = 4.1 \times 10^3 \frac{R_{10}^{1/4} E_{51}^{0.016} M_c^{0.03} \kappa_{0.2}^{0.27}}{f_p^{0.022}} t_{day}^{-0.47} \text{ K.} \quad (2)$$

For the K10 model,

$$L(t) = 2.0 \times 10^{40} \frac{R_{10} M_c^{1/4} v_9^{7/4}}{\kappa_{0.2}^{3/4}} t_{day}^{-0.5} \text{ erg s}^{-1}$$

$$T_{eff}(t) = 5.3 \times 10^3 \frac{R_{10}^{1/4}}{\kappa_{0.2}^{35/36}} t_{day}^{-37/72} \text{ K.} \quad (3)$$

Here, R_{10} is the radius of the progenitor or the companion star ($R_* = (\text{separation distance})/2$ for the K10 model) in units of 10^{10} cm, E_{51} is the explosion energy $E = E/10^{51}$ erg, M_c is the progenitor (or the ejecta) mass in units of $1.4 M_\odot$, $\kappa_{0.2}$ is the opacity in units of $0.2 \text{ cm}^2 \text{ g}^{-1}$, f_p is the form factor that ranges between 0.031 and 0.13 (Calzabara & Matzner 2004; RW11), and v_9 is the expansion velocity of the ejecta in units of 10^9 cm s^{-1} . For the RW11 model, we adopt $M_c = 1/1.4$, $E_{51} = M_c$, $\kappa_{0.2} = 1$, and $f_p = 0.05$. For the K10 model, we adopt $M_c = 1/1.4$, $\kappa_{0.2} = 1$, and $v_9 = 1$. Note that the K10 prediction is anisotropic and the strength of the signal varies with viewing angle. The K10 curve in Eq. (3) describes the case with a viewing angle that gives nearly maximal observable signal of the shock-heated cooling emission (“optimal viewing angle”). We define the ”common viewing angle” as the angle that corresponds roughly to an 80 percentile of the viewing angle where the observed signal is 10% of the signal under the optimal viewing angle (Bloom et al. 2012). To model the common viewing angle case, we simply scaled the optimal viewing angle prediction by a factor of 10.

These theoretical light curves are plotted in Figure 3 for several different values of t_d that range from 0.5 to 2.5 days, and for a range of R_* values. In Figure 4, the theoretical light curves are plotted assuming $t_d = 1.6$ days, where the RW11 model is for $0.1 R_\odot$ (the dashed lines), and the K10 model (the dotted lines) is for $0.1 R_\odot$ (an optimal viewing angle), $1 R_\odot$ and $2 R_\odot$ (a common viewing angle).

We find that the observed signal can be explained with a variety of progenitor systems. With the RW11 model, a progenitor radius of $\sim 0.1 R_\odot$ fits the data well, which is consistent with a DD system that undergoes a prompt detonation (Pakmor et al. 2012; Tanikawa et al. 2015) and a SD system where the white dwarf is a recurrent nova with rapid mass accretion of hydrogen-rich matter (e.g., Hachisu & Kato 2003). On the other hand, this result is inconsistent with a DD system with a long-delayed explosion (Yoon et al. 2007) and with a SD system where the white dwarf radius is predicted as small as $R_* \lesssim 0.01 R_\odot$ at the shock breakout (Hoflich et al. 2009; Yoon & Langer 2004; Woosley & Kasen 2011). For the K10

model, the result can be explained by a SD system with a companion star with $R_* = 0.1 - 1 R_\odot$, where $R_* = 0.1 R_\odot$ is for an optimal viewing angle, and $R_* \sim 1 R_\odot$ for a more common viewing angle. This result excludes cases where a companion star has $R_* \gg 1 R_\odot$ like that of a subgiant of a red giant star.

5. UPPER LIMITS ON R_*

Clearly, our constraints on R_* depends critically on how significant the detected signal is. Alternatively, we can take a more conservative approach of considering $3-\sigma$ upper limits only to place a limit on R_* . With the upper limits that extend to several days before the first detection, we can still provide a meaningful constraint on the progenitor system that is largely independent of t_d .

Using Eqs. (2) and (3), we calculated R_* values for $3-\sigma$ limits at epochs that follows an assumed explosion time. The smallest value among such R_* values, is taken to be an upper limit on R_* , $R_{*,\text{up}}$. When $R_* \lesssim 1 R_\odot$, the light curve peak of the shock-heated cooling emission appears within 1 day of the explosion (Figure 4), so $R_{*,\text{up}}$ is determined by a $3-\sigma$ upper limit that is closest in time to the assumed explosion time in such a case.

We also need to consider $R_{*,\text{min}}$, the minimal radius that one can probe with a given set of time series observation. This is necessary since the shock-heated cooling emission can drop suddenly when the diffusion wave reaches material where the gas pressure dominates the radiation pressure (Rabinak et al. 2011, 2012). This limits the duration of the shock-heated cooling curve in such a way that the larger the progenitor is, the longer the duration becomes. For a given time t since the explosion, the size of the progenitor for which the light curve drop suddenly at t can be given as

$$R_{*,\text{min}} \simeq 0.013 E_{51}^{-0.66} M_c^{0.56} f_{0.05}^{0.15} t_{4hr} R_\odot, \quad (4)$$

where t_{4hr} is time in units of 4hr (RW11; Bloom et al. 2012). For one day cadence observation, we are limited to probing $R_* > R_{*,\text{min}} \sim 0.07 R_\odot$.

In Figure 5, we show $R_{*,\text{up}}$, and $R_{*,\text{min}}$ as a function of the assumed explosion time for which the time of the first detection of the radioactively powered light curve is set to 0. For $R_{*,\text{up}}$, we used the RW11 model (the dashed line), and the K10 model for two cases – one for an optimal viewing angle to detect the shock-heated cooling emission (the dotted line), and another for a much less optimal viewing angle that produces about 10% of the observed emission under an optimal viewing angle (the dot-dashed line). At a given time, the larger value between $R_{*,\text{up}}$ and $R_{*,\text{min}}$ can be taken as the constraint on the progenitor size. The figure shows sawtooth-like curves for both $R_{*,\text{max}}$ and $R_{*,\text{min}}$, which result from the cadence

of our data points. The constraint on R_* is the strongest when the explosion time is near our data points in such a way that the maximum of the light curve coincides with the epochs where the data were taken. As we noted earlier, the explosion time is most likely at between the first light time of a single power-law fit and a few days before it. In such cases, we find that R_* stays at $R_* \lesssim 0.1 R_\odot$ for fluxes coming from a progenitor star (RW11) or interaction with a companion star at an optimal viewing angle. For the K10 model with a less optimal viewing angle, we find that $R_* \lesssim 1 R_\odot$. If the explosion time falls between the first detection time and one day before it, then the constraint on the progenitor system becomes about 10 times weaker. These limits are in agreement with the inferred progenitor size from the possible shock-heated cooling emission as discussed in the previous section.

The constraint of $R_* \lesssim 0.1 R_\odot$ excludes many possible SN Ia progenitors. As discussed in Bloom et al. (2012), H-burning or He-burning MS stars with $M = 0.5 - 3.0 M_\odot$ would have radii of $R_* > 0.2 R_\odot$ and can be excluded. C-burning MS stars are expected to have $M > M_\odot$ (Boozer et al. 1973), and many such stars can be excluded when $M > 2 M_\odot$.

A useful constraint on a companion star can be obtained too. Our result suggests that the radius of a companion star should be $R_* \lesssim R_\odot$ even if the viewing angle is not in an optimal direction. This excludes red giant stars with 1-2 M_\odot that would have radii $R_* \gtrsim 100 R_\odot$. MS sub-giants with 5 – 6 M_\odot would have radii $R_* \sim 10 R_\odot$, and they can be excluded too. MS stars with $\sim 1 M_\odot$ are consistent with our limit.

6. CONCLUSION

In this paper, we presented the light curve of a SN Ia, SN 2015F, between -84 and 41 days with respect to the first light time. Our data caught the rise of SN 2015F at a daily cadence, providing an estimate of the first light time of 1.6 days before the first detection (single power-law fit). Through our light curve analysis, we determined the distance to NGC 2442 and SN 2015F to be 23.9 ± 0.4 Mpc, and the reddening parameter of $E(B-V) = 0.035 \pm 0.033$.

More importantly, we detected a possible signal from shock-heated cooling emission at -3 and -2 days prior to the first detection of the radioactively powered light. Additionally, we obtained upper limits for any precursor emission over 40 nights before the first detection. The possible detection of the shock-heated cooling emission places stringent limits on the SN 2015F progenitor, allowing a $R_* \sim 0.1 R_\odot$ progenitor system (such as in a prompt detonation of a DD system), or companion stars with $R_* \simeq 0.1 - 1 R_\odot$ in a SD system. On the other hand, the possible detection and the upper limits around and before the first light time exclude a very small progenitor with $R_* \ll 0.1 R_\odot$, large progenitors with $R_* \gg 0.1 R_\odot$ or a

very large companion star with $R_* \gg R_\odot$, and these conclusions are largely independent on the exact time of the explosion time.

The detected shock-heated cooling emission is at a level of $R = 21$ mag at ~ 20 Mpc and with various kinds of extinctions along the line of sight ($M_R = -11$ mag). This detection, although marginal ($> 97.4\%$), indicates that high cadence observation of SNe Ia is a very promising way to probe their progenitor systems that have been elusive in the previous searches. A secure detection of such a signal requires a sensitivity only a few times better than this work, which can be easily achieved with observations using 1-m class telescopes (e.g., Lee et al. 2010).

This work was supported by the Creative Initiative program, No. 2008-0060544, of the National Research Foundation of Korea (NRFK) funded by the Korean government (MSIP). This paper includes the data taken at the Siding Spring Observatory in Australia. We thank the anonymous referee for useful comments.

REFERENCES

- Bertin, E., & Arnouts, S. 1996, *A&AS*, 117, 393
- Bloom, J. S., Kasen, D., Shen, K. J., et al. 2012, *ApJ*, 744, L17
- Boozer, A. H., Joss, P. C., & Salpeter E. E. 1973, *ApJ*, 181, 393
- Cao, Y., Kulkarni, S. R., Howell, D., et al. 2015, *Nature*, 521, 328
- Calzavara, A. J., & Matzner, C. D. 2004, *MNRAS*, 351, 694
- Feldmeier, J. J., Ciardullo, R., & Jacoby, G. H. 1996, *ApJ*, 461, L25
- Foley, R. J., Challis, P. J., Filippenko, A. V., et al. 2012, *ApJ*, 744, 38
- Fraser, M., Smith, M., Firth, R., et al. 2015, *ATel*, #7209
- Goobar, A., Kormer, M., Siverd, R., et al. 2015, *ApJ*, 799, 106
- Goobar, A., Johansson, J., Amanullah, R., et al. 2014, *ApJ*, 784, L12
- Hachinger, S., et al. 2013, *MNRAS*, 429, 2228
- Hachisu, I., & Kato, M. 2003, *ApJ*, 588, 1003
- Henden, A. A., Levine, S. E., Terrell, D., Smith, T. C., and Welch, D. 2012, *JAVSO*, 40, 430
- Hillebrandt, W., & Niemeyer, J. C. 2000, *ARA&A*, 38, 191
- Höflich, P., & Schaefer, B. E. 2009, *ApJ*, 705, 483
- Hoyle, F., Fowler, W. A. 1960, *ApJ*, 132, 565
- Im, M., Choi, C., & Kim, K., 2015, *Journal of Korean Astronomical Society*, 48, 207
- Im, M., Ko, J., Cho, Y., et al. 2010, *Journal of Korean Astronomical Society*, 43, 75
- Jeon, Y., Im, M., Ibrahimov, M., Lee, H. M., Lee, I., & Lee, M. G. 2010, *ApJS*, 190, 166
- Jha, S., Riess, A. G., & Kirshner, R. P. 2007, *AJ*, 659, 122
- Kasen, D. 2010, *ApJ*, 708, 1025
- Kessler, R., Bernstein, J. P., Cinabro, D., et al. 2009, *PASP*, 121, 1028
- Kutsuna, M., & Shigeyama, T. 2015, *PASJ*, 67, 5414

- Lee, I., Im, M., & Urata, Y. 2010, *Journal of Korean Astronomical Society*, 43, 95
- Lee, M. G., & Jang, I. S. 2012, *ApJ*, 760, L14
- Macri, L.M., Calzetti, D., Freedman, W. L., et al. 2001, *ApJ*, 549, 721
- Maeda, K., Kutsuna, M., & Shigeyama, T. 2014 *ApJ*, 794, 37
- Maoz, D., Mannucci, F., & Nelemans, G. 2014, *ARA&A*, 52, 107
- Matheson, T., Joyce, R. R., Allen, L. E., et al. 2012, 754, 19
- Mazzali, P. A., Sullivan, M., Hachinger, S., et al. 2014, *MNRAS*, 439, 1959
- McCully, C., Jha, S. W., Foley, R. J., et al. 2014, *Nature*, 512, 54
- Munari, U., Henden, A., Belligol, R., et al. 2013, *NewA*, 20, 30
- Nakar, E., & Sari, R. 2010, *ApJ*, 725, 904
- Nugent, P. E., Sullivan, M., Cenko, S. B., et al. 2011, *Nature*, 480, 344
- Olling, R. P., Mushotsky, R., Shaya, E. J., et al. 2015, *Nature*, 521, 332
- Pakmor, R., Kromer, M., Taubenberger, S., Sim, S. A., Ropke, F. K., & Hillenbrandt, W. 2012, *ApJ*, 747, L10
- Pan, K.-C., Ricker, P. M., & Taam, R. E. 2012, *ApJ*, 750, 151
- Patat, F., Cordiner, M. A., Cox, N. L. J., et al. 2013, *A&A*, 549, 62
- Piro, A. L., & Nakar, E. 2014, *ApJ*, 784, 85
- Piro, A. L., & Nakar, E. 2013, *ApJ*, 769, 67
- Piro, A. L., Chang, P., & Weinberg, N. N. 2010, *ApJ*, 708, 598
- Rabinak, I., Livne, E., & Waxman, E. 2012, *ApJ*, 757, 35
- Rabinak, I., & Waxman, E. 2011, *ApJ*, 728, 63
- Richmond, M. W., & Smith, H. A. 2012, *JAVSO*, 40, 872
- Rizzi, L., Tully, R. B., Makarov, D., et al. 2007, *ApJ*, 661, 815
- Sakai, S., Ferrarese, L., Kennicutt, R. C., Jr., & Saha, A. 2004, *ApJ*, 608, 42

- Shappee, B. J., Piro, A. L., Holoiien, T. W.-S., et al. 2015, ApJ, submitted
- Shappee, B. J., & Stanek, K. Z. 2011, ApJ, 733, 124
- Schlafly, E. F., & Finkbeiner, D. P. 2011, ApJ, 737, 103
- Silverman, J. M., Ganeshalingam, M., Cenko, S. B., et al. 2012, ApJ, 756, L7
- amman, G. A., & Reindl, B. 2013, A&A, 549, 136
- Tanikawa, A., Nakasato, N., Sato, Y., Nomoto, K., Maeda, K., Hachisu, I. 2015, ApJ, in press
- Tsvetkov, D. Y., Shugarov, S. Y., Volkov, I. M., et al. 2013, CoSKA, 43, 94
- Tully, R. B., Rizzi, L., Shaya, E. J., et al. 2009, AJ, 138, 323
- Tully, R. B. 1988, Nearby Galaxies Catalog (Cambridge: CUP)
- Urata, Y., Huang, K., Im, M., et al. 2009, ApJ, 706, L183
- Vinko, J., Sarneczky, K., Takats, K., et al. 2012, A&A, 546, 12
- Woosley, S. E., & Kasen, D. 2011, ApJ, 734, 38
- Yamanaka, M., Maeda, K., Kawabata, M., et al. 2014, ApJ, 782, L35
- Yoon, S.-C., Podsiadlowski, P., & Rosswog, S. 2007, MNRAS, 380, 933
- Yoon, S.-C., & Langer, N. 2004, A&A, 419, 645
- Zheng, W., Shivvers, I., Filippenko, A. V., et al. 2014, ApJ, 783, L24
- Zheng, W., Silverman, J. M., Filippenko, A. V., et al. 2013, ApJ, 778, L15

Table 1. Long-term Light Curve Fitting Results

$t_{\max}(B)$ (JD)	Δ	$\Delta m_{15}(B)$ (Mag)	B_{\max} (Mag)	$M_{B,\max}$ (Mag)	μ	t_{rise} (Days)	$E(B - V)_{\text{host}}$ (Mag)
$2,457,106.48 \pm 0.09$	0.11 ± 0.04	1.26 ± 0.10	13.36 ± 0.10	-19.42 ± 0.11	31.89 ± 0.04	$17.5 \pm 0.6^{\text{a}}$	0.035 ± 0.033

Note. — ^a The error indicates a possible range in t_{rise} , which reflects the large uncertainty in the first light time as discussed in Section 3.2.

Table 2. *R*-band Light Curve

UT Date 2015	Phase ^a (Days)	F_ν (μJy)	Error (μJy)
Dec 14.6146	-83.8480	-1.27	2.22
Dec 15.6540	-82.8086	-4.20	5.07
Dec 16.6511	-81.8115	-6.90	2.30
Dec 18.6542	-79.8084	6.09	3.03
Dec 19.7066	-78.7560	-2.78	5.92
Dec 20.6428	-77.8198	7.28	3.06
Dec 21.6767	-76.7859	0.61	6.17
Dec 31.5655	-66.8971	-0.62	4.95
Jan 07.6148	-59.8478	-0.29	4.27
Jan 08.5116	-58.9510	1.70	3.57
Jan 15.7366	-51.7260	-8.58	5.27
Jan 16.6335	-50.8291	-3.02	2.71
Jan 17.6600	-49.8026	4.55	4.29
Jan 18.6244	-48.8382	4.05	4.02
Jan 23.5471	-43.9155	-1.46	2.09
Jan 29.5524	-37.9102	-0.04	2.81
Jan 30.5336	-36.9290	6.96	3.65
Jan 31.6084	-35.8542	-4.02	4.97
Feb 01.4900	-34.9726	-12.15	4.52
Feb 04.5529	-31.9097	-7.81	6.94
Feb 07.5780	-28.8846	-5.60	3.97
Feb 08.5681	-27.8945	4.53	9.35
Feb 09.5751	-26.8875	-14.72	6.88
Feb 10.5929	-25.8697	0.53	5.45
Feb 11.5777	-24.8849	-1.36	6.46
Feb 13.6005	-22.8621	0.97	4.97
Feb 15.5596	-20.9030	0.98	3.61
Feb 16.5984	-19.8642	10.97	9.33
Feb 18.5182	-17.9444	2.74	3.18
Feb 19.5996	-16.8630	-2.24	5.31

Table 2—Continued

UT Date 2015	Phase ^a (Days)	F_ν (μ Jy)	Error (μ Jy)
Feb 21.4670	-14.9956	1.23	4.11
Feb 22.5007	-13.9619	4.88	2.91
Feb 23.5556	-12.9070	2.37	2.11
Feb 26.4913	-9.9713	-2.24	3.02
Mar 02.4899	-5.9727	0.75	6.69
Mar 03.5667	-4.8959	0.39	22.67
Mar 04.5186	-3.9440	-4.98	5.09
Mar 05.5475	-2.9151	15.73	7.65
Mar 06.5386	-1.9240	11.91	4.71
Mar 07.5108	-0.9518	4.77	5.74
Mar 08.4626	0.0000	114.08	12.76
Mar 08.4649	0.0023	126.01	13.00
Mar 08.4672	0.0046	119.56	12.33
Mar 09.4553	0.9927	358.43	14.01
Mar 09.4577	0.9951	356.78	15.11
Mar 09.4600	0.9974	378.09	15.19
Mar 09.5398	1.0772	438.13	23.31
Mar 09.5421	1.0795	392.65	20.46
Mar 09.5445	1.0819	389.40	23.68
Mar 09.7901 ^b	1.3275	448.75	30.69
Mar 11.4424	2.9798	1341.53	72.83
Mar 11.4449	2.9823	1379.11	59.89
Mar 11.4474	2.9848	1424.30	60.31
Mar 11.4963	3.0337	1441.45	37.56
Mar 11.4988	3.0362	1404.75	35.08
Mar 11.5014	3.0388	1421.67	35.50
Mar 11.8010 ^b	3.3384	1519.15	61.03
Mar 14.7630 ^b	6.3004	4733.69	215.86
Mar 15.7460 ^b	7.2834	6338.69	227.11
Mar 16.4303	7.9677	7613.77	181.86

Table 2—Continued

UT Date 2015	Phase ^a (Days)	F_ν (μJy)	Error (μJy)
Mar 16.4327	7.9701	7578.79	181.03
Mar 16.4352	7.9726	7516.23	179.53
Mar 16.5189	8.0563	7741.05	184.90
Mar 16.5213	8.0587	7762.47	185.42
Mar 16.5237	8.0611	7812.68	186.62

Note. — ^a Days from the first detection of radioactively powered emission on 2015 March 8.46 (JD 2,457,089.9626).

^b Data taken in South Africa (Monard). All the other data come from LSGT observation.

Emergence of SN 2015F in NGC 2442

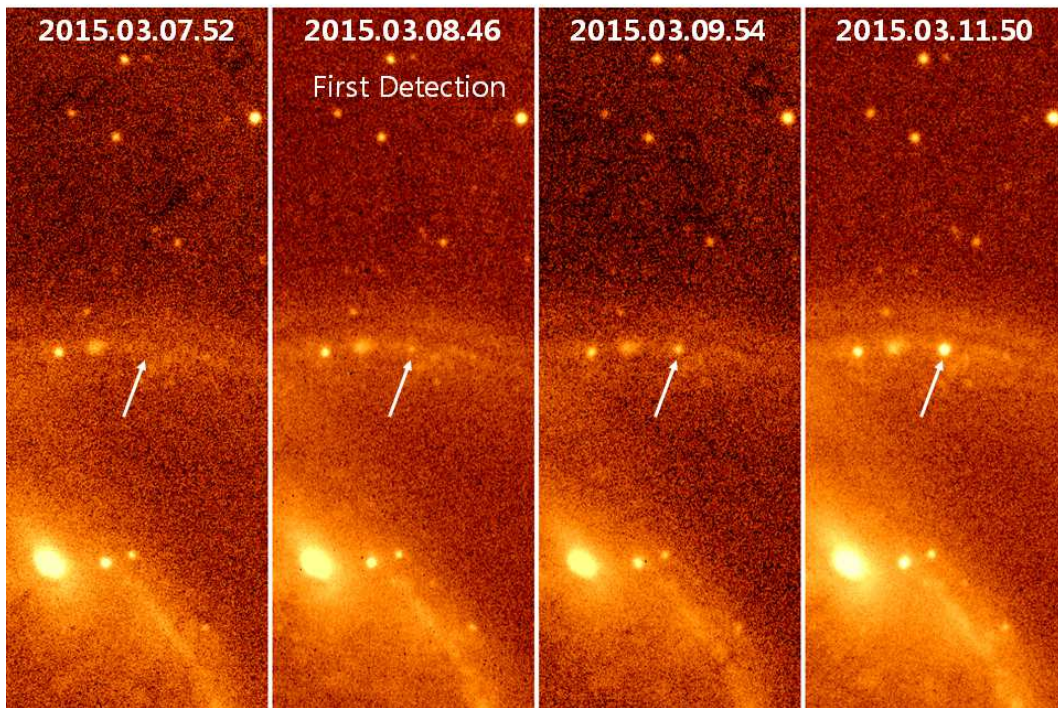


Fig. 1.— The R -band images of SN 2015F taken with LSGT, before the first detection of the radioactively powered emission (the leftmost) and after. Indicated in the figure are the UT-date of the observation, and the location of SN 2015F.

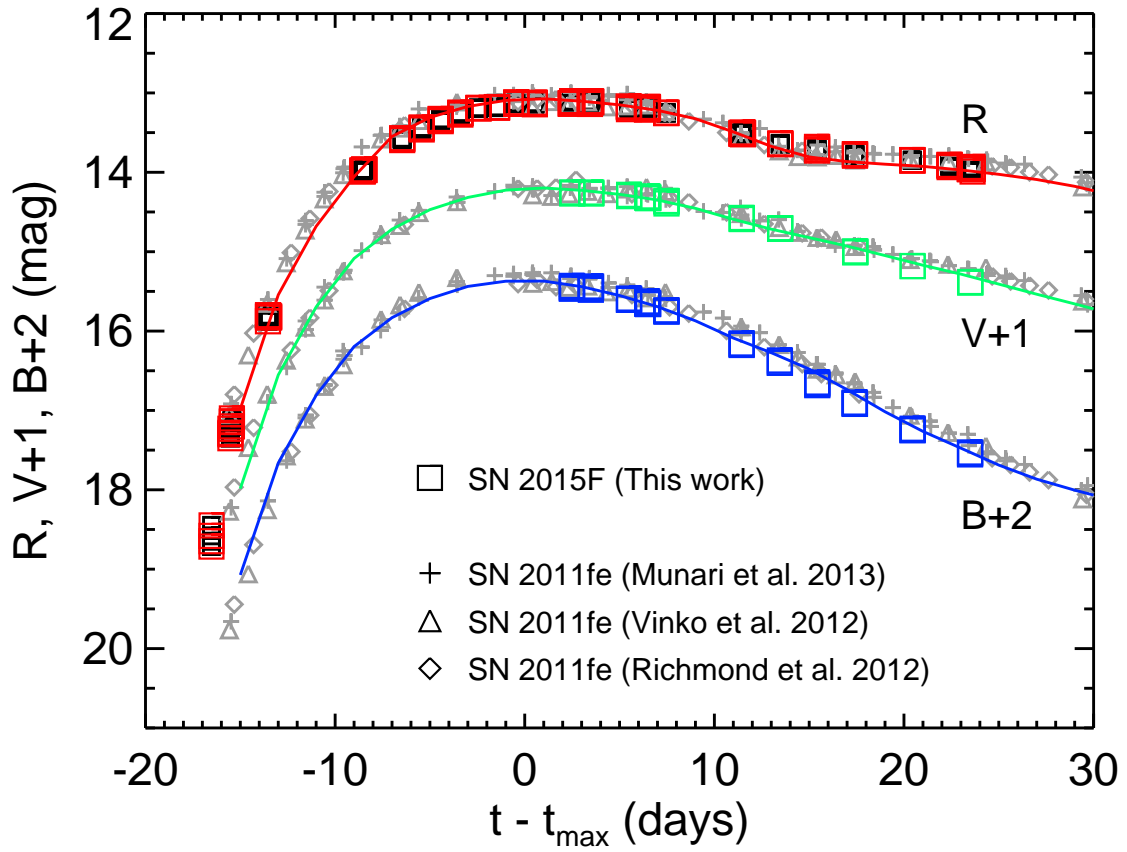


Fig. 2.— The long-term light curve of SN 2015F up to 22 days after the *B*-band maximum, along with the best-fit models and the SN 2011fe data points. The SN 2015F light curve suggests that it is a typical SN Ia, very similar in properties to SN 2011fe.

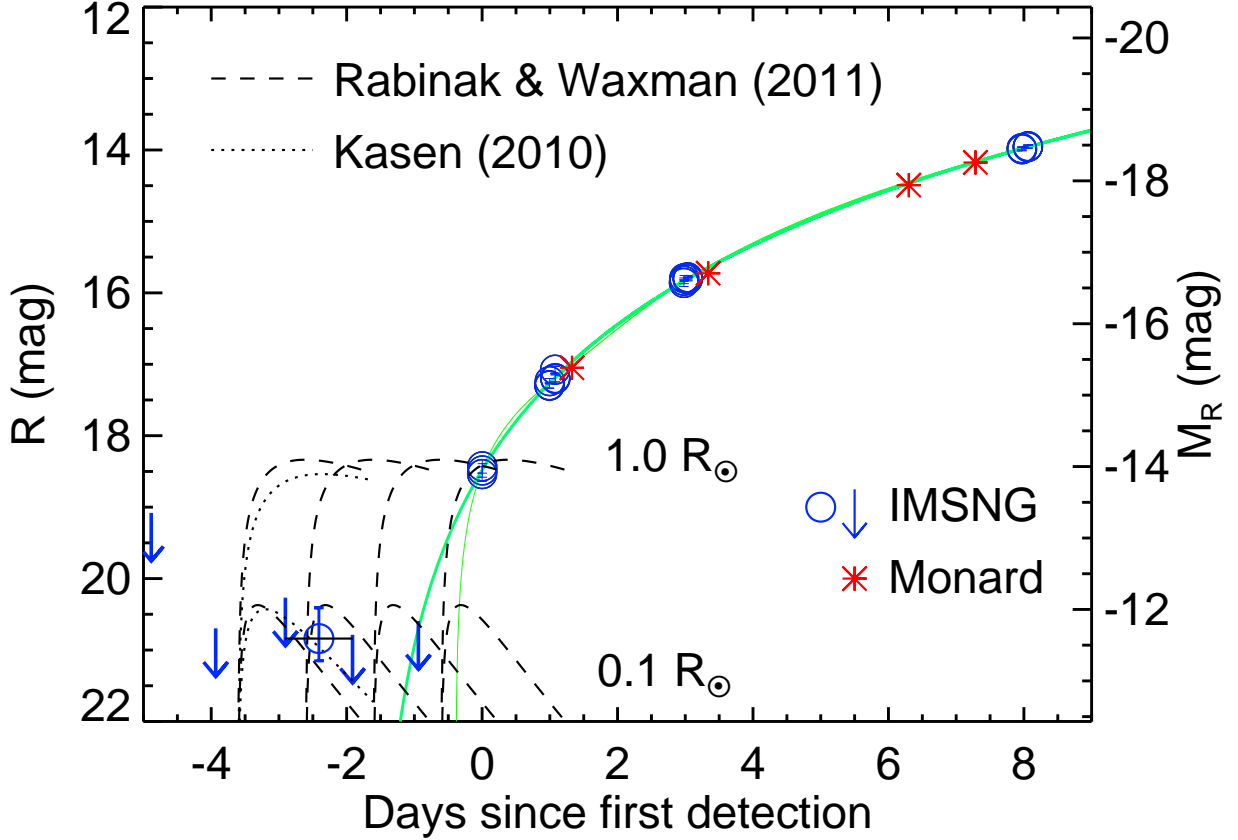


Fig. 3.— The R -band light curve of SN 2015F at the epochs between -5 days and $+8$ days from the first detection. The blue circles and arrows ($3\text{-}\sigma$ upper limits) are for the LSGT observations and the red asterisks are for the data taken at South Africa. The average of the possible detections of shock-heated cooling emission is plotted at -3 days (see Figure 4 and text for more detail). The green solid lines indicate the best-fit results from a single power-law (thick) and a broken power-law (thin) fits. The dashed and the dotted lines are the predictions of two models (RW11 and K10) of shock-heated cooling light curves for two progenitor star radii (for the K10 model, the size of a companion star) of 0.1 and $1 R_{\odot}$. The model curves are plotted for four different explosion times at -0.5 , -1.5 , -2.5 , and -3.5 days. The K10 model is for a viewing angle that is favorable to detect the early emission.

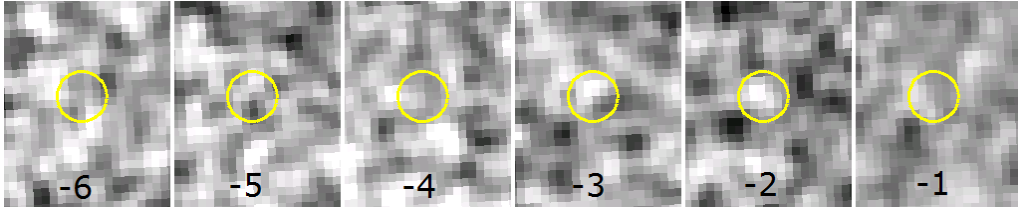
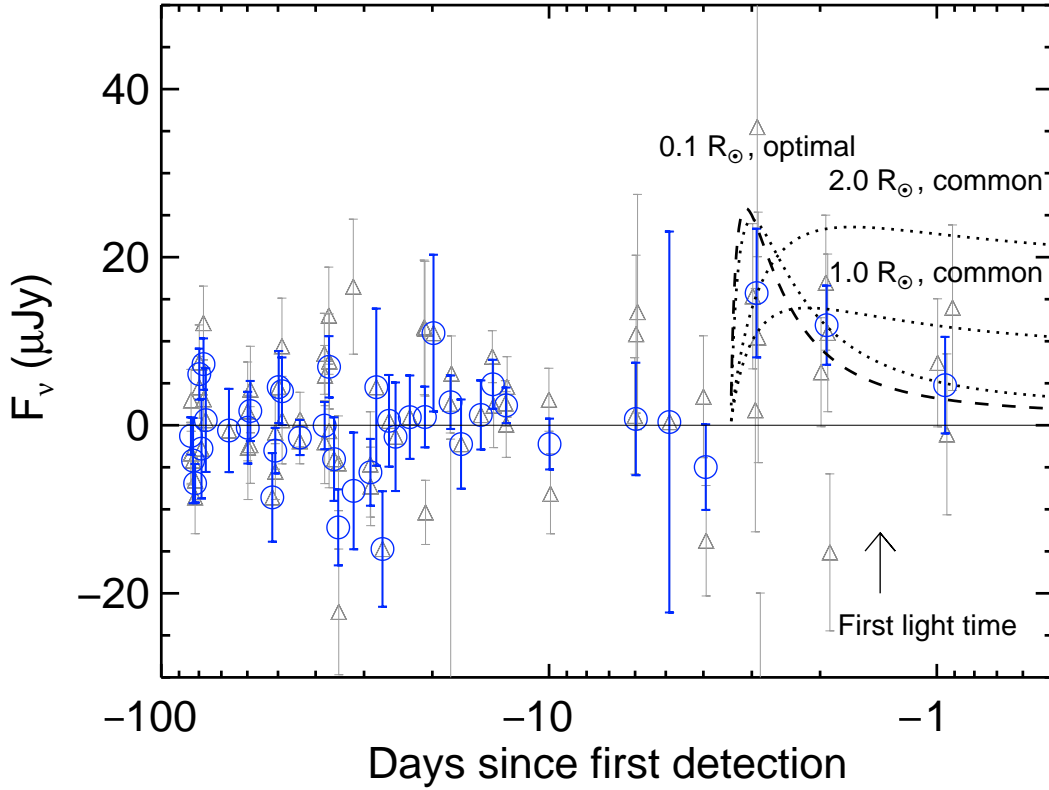


Fig. 4.— Possible detection of the early emission from shock-heated materials of SN 2015F. Top: The light curve from an aperture photometry ($3''$ diameter) that is performed at the SN 2015F location before and around the first light time. The blue circles are the results from a stacked image of all images taken at each night, and gray triangles are for measurements made on images taken at several different epochs each night (cadence of ~ 1.5 hr). Two notable events are recorded over two consecutive nights at -3 and -2 days, each with a $2\text{-}\sigma$ significance. The RW11 (dashed line) and the K10 (dotted line) model predictions are shown for several different progenitor sizes. For the K10 model, we plot the predictions for $R_* = 0.1 R_\odot$ under an optimal viewing angle, and $R_* = 1$ and $2 R_\odot$ under a common viewing angle. The signals at -3 and -2 days, if real, can be explained with a SD system having a companion star with $R_* \simeq 0.1 - 1.0 R_\odot$ or a prompt explosion of a DD system ($R_* \sim 0.1 R_\odot$). This result excludes a companion star with $R_* \gg 1 R_\odot$ such as that of a subgiant or a red giant star, or a very small progenitor with $R_* \lesssim 0.01 R_\odot$ such as in a delayed detonation of a DD system. The first light time estimate from a single power-law fit is shown at -1.6 days. Bottom: The difference images at the location of the SN 2015F which is marked with a $3''$ diameter yellow circle. The numbers in each panel shows the number of days before the first detection. The images are convolved with a $\sigma = 1$ pixel Gaussian kernel.

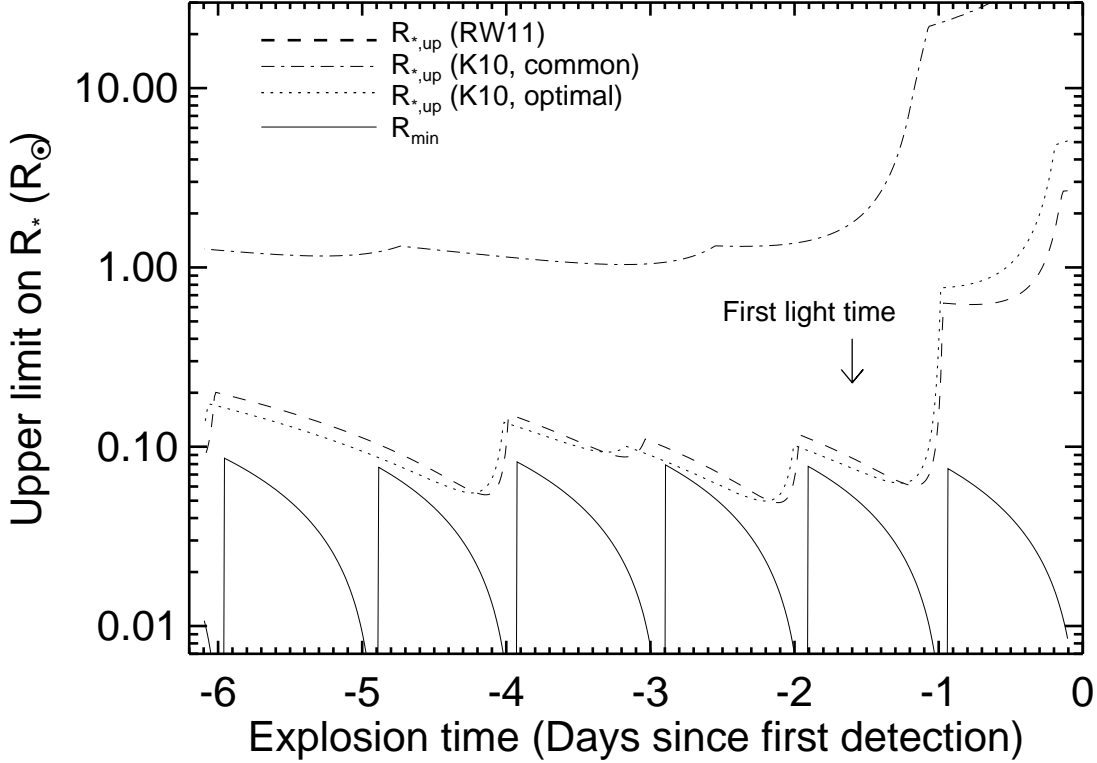


Fig. 5.— The upper limits on the progenitor radius as a function of the assumed explosion time. The dashed line indicates the upper limits from the shock-heated cooling light curve of RW11, and the the solid line represents the minimal radius we can explore with our data cadence. We also plot the upper limits from the K10 model for an optimal (dotted line) and a more common viewing angle (dot-dashed line). The first light time from a single power-law fitting is indicated at -1.6 days. These limits exclude a very large progenitor system ($R_* \gg 1 R_\odot$) unless the first light time is located within one day from the first detection time.